



**HAL**  
open science

# Exploring the Cloud Top Phase Partitioning in Different Cloud Types Using Active and Passive Satellite Sensors

Olimpia Bruno, Corinna Hoose, Trude Storelvmo, Quentin Coopman, Martin Stengel

## ► To cite this version:

Olimpia Bruno, Corinna Hoose, Trude Storelvmo, Quentin Coopman, Martin Stengel. Exploring the Cloud Top Phase Partitioning in Different Cloud Types Using Active and Passive Satellite Sensors. *Geophysical Research Letters*, 2021, *Geophysical Research Letters*, 48 (2), 10.1029/2020gl089863 . hal-04680901

**HAL Id: hal-04680901**

**<https://hal.univ-lille.fr/hal-04680901v1>**

Submitted on 29 Aug 2024

**HAL** is a multi-disciplinary open access archive for the deposit and dissemination of scientific research documents, whether they are published or not. The documents may come from teaching and research institutions in France or abroad, or from public or private research centers.

L'archive ouverte pluridisciplinaire **HAL**, est destinée au dépôt et à la diffusion de documents scientifiques de niveau recherche, publiés ou non, émanant des établissements d'enseignement et de recherche français ou étrangers, des laboratoires publics ou privés.



Distributed under a Creative Commons Attribution - NonCommercial 4.0 International License

# Geophysical Research Letters



## RESEARCH LETTER

10.1029/2020GL089863

### Key Points:

- Despite phase and temperature mismatches, the retrievals based on passive and active satellite sensors qualitatively agree on the following
- Supercooled liquid fraction is larger in the Southern Hemisphere than in the Northern Hemisphere, except for continental low-level clouds
- In clouds with temperatures from  $-40^{\circ}\text{C}$  to  $0^{\circ}\text{C}$  at the same height-level, supercooled liquid fraction increases with cloud optical thickness

### Supporting Information:

- Supporting Information S1

### Correspondence to:

O. Bruno,  
[olimpia.bruno@kit.edu](mailto:olimpia.bruno@kit.edu)

### Citation:

Bruno, O., Hoose, C., Storelvmo, T., Coopman, Q., & Stengel, M. (2021). Exploring the cloud top phase partitioning in different cloud types using active and passive satellite sensors. *Geophysical Research Letters*, 48, e2020GL089863. <https://doi.org/10.1029/2020GL089863>





Received 4 AUG 2020

Accepted 4 DEC 2020

© 2020. The Authors.

This is an open access article under the terms of the [Creative Commons Attribution-NonCommercial License](https://creativecommons.org/licenses/by/4.0/), which permits use, distribution and reproduction in any medium, provided the original work is properly cited and is not used for commercial purposes.

## Exploring the Cloud Top Phase Partitioning in Different Cloud Types Using Active and Passive Satellite Sensors

Olimpia Bruno<sup>1</sup> , Corinna Hoose<sup>1</sup> , Trude Storelvmo<sup>2</sup> , Quentin Coopman<sup>1</sup> , and Martin Stengel<sup>3</sup> 

<sup>1</sup>Institute of Meteorology and Climate Research, Karlsruhe Institute of Technology, Karlsruhe, Germany, <sup>2</sup>Department of Geosciences, University of Oslo, Oslo, Norway, <sup>3</sup>Deutscher Wetterdienst, Offenbach am Main, Germany

**Abstract** One of the largest uncertainties in numerical weather prediction and climate models is the representation of mixed-phase clouds. With the aim of understanding how the supercooled liquid fraction (SLF) in clouds with temperature from  $-40^{\circ}\text{C}$  to  $0^{\circ}\text{C}$  is related to temperature, geographical location, and cloud type, our analysis contains a comparison of four satellite-based datasets (one derived from active and three from passive satellite sensors), and focuses on SLF distribution near-globally, but also stratified by latitude and continental/maritime regions. Despite the warm bias in cloud top temperature of the passive sensor compared to the active sensor and the phase mismatch in collocated data, all datasets indicate, at the same height-level, an increase of SLF with cloud optical thickness, and generally larger SLF in the Southern Hemisphere than in the Northern Hemisphere (up to about 20% difference), with the exception of continental low-level clouds, for which the opposite is true.

**Plain Language Summary** In mixed-phase clouds, hydrometeors consisting of ice and supercooled liquid water (i.e., water below  $0^{\circ}\text{C}$ ) can exist simultaneously. In the mixed-phase temperature range ( $-40^{\circ}\text{C}$  to  $0^{\circ}\text{C}$ ), ice-nucleating particles (e.g., mineral dusts, biological aerosol particles) are needed for glaciation to be possible. The partitioning into liquid and ice depends not only on the ice-nucleating particles, but also, for example, on cloud dynamics and ice multiplication processes, influencing in turn the lifetime and the precipitation type of these clouds, and the Earth-atmosphere energy balance locally and globally. In this study, we show ice and liquid partitioning for different cloud types, comparing four satellite-based datasets. This allows us to identify robustly their common trends despite their differences. Our results show on average less ice in the Northern than in the Southern Hemisphere when considering all clouds together, and that the larger the cloud optical thickness, the less ice when treating the cloud types separately. The partitioning of cloud types over sea and over land in both hemispheres show less ice in the Southern than in the Northern Hemisphere for high-level and mid-level clouds, but the opposite for low-level clouds over land. This might be due to differences in aerosol composition and distribution.

## 1. Introduction

Mixed-phase clouds, i.e., clouds in which ice particles and supercooled liquid water can coexist in the temperature range of approximately  $-40^{\circ}\text{C}$  to  $0^{\circ}\text{C}$ , are not fully understood yet and therefore not well represented in weather and climate models (Forbes & Ahlgrimm, 2014; McCoy et al., 2016).

Several studies have shown that mixed-phase clouds occur irrespective of the season, can be found in diverse locations, and can be associated with various cloud types (Korolev et al., 2017). Observations of mixed-phase clouds include active (e.g., Cesana & Storelvmo, 2017; Tan et al., 2014; Zhang et al., 2010) and passive satellite (e.g., Coopman et al., 2019; Noh et al., 2019; Tan et al., 2019), airborne in situ (e.g., Barrett et al., 2020; Costa et al., 2017; Korolev, 2008), ground-based (e.g., Gierens et al., 2020; Henneberger et al., 2013; Yu et al., 2014) and aircraft-based remote sensing measurements (e.g., Plummer et al., 2014; Wang et al., 2012). In Tan et al. (2014), in particular, mixed-phase clouds have been studied statistically in terms of supercooled cloud fraction, defined as the ratio of the in-cloud frequency of supercooled liquid pixels to the total frequency of supercooled liquid and ice pixels within  $2^{\circ}$  latitude by  $5^{\circ}$  longitude grid boxes, at several isotherms between  $-10^{\circ}\text{C}$  and  $-30^{\circ}\text{C}$ , distinguishing cases in the Northern Hemisphere (NH) and in the Southern Hemisphere (SH), as well as cases over ocean and over land. This study consisted of the analysis of about 5 years of data from NASA's spaceborne lidar, CALIOP (Cloud-Aerosol Lidar with

Orthogonal Polarization) level 2 Vertical Feature Mask (VFM) in versions 3.01 and 3.02, and the relationship between the cloud phase and several aerosol types was determined. They found that dust aerosols might strongly influence the supercooled cloud fraction by acting as ice-nucleating particles (INPs), illustrating how important the atmospheric aerosol composition can be for the cloud phase. Moreover, a larger supercooled cloud fraction in SH than in NH has been found, which may be caused by the presence of more land in the NH, where efficient INPs originate. This result may also explain why a larger supercooled cloud fraction has been found over ocean than over land.

As in Tan et al. (2014), we apply a statistical approach to quantify the phase distribution of mixed-phase clouds on isotherms. In addition, we use the International Satellite Cloud Climatology Project (ISCCP) cloud classification (Rossow & Schiffer, 1999) to distinguish different cloud types. Our study includes data from passive (Advanced Very High-Resolution Radiometer—AVHRR) and active (Cloud-Aerosol Lidar and Infrared Pathfinder Satellite Observation—CALIPSO) satellite sensors, with the intention to identify robust signals despite differences, facilitating the potential identification of common features based on different sources and algorithms. Passive sensors offer the benefit of long-period records with daily near-global coverage, which motivates us to compare three AVHRR-based datasets with the CALIPSO-based dataset, and to present this work as a validation study.

After a description of the datasets and the method in Sections 2 and 3 contains the analysis and the results of our study, while discussion and conclusions are presented in Section 4.

## 2. Datasets and Method

### 2.1. Datasets

The datasets we analyze are Cloud\_cci AVHRR-PMv2 (Stengel et al., 2017), Cloud\_cci AVHRR-PMv3 (Stengel et al., 2020), CLARA-A2 (Karlsson et al., 2017), and CALIOP V4 (Liu et al., 2019). While the first three are based on the polar-orbiting passive satellite sensor AVHRR onboard NOAA satellites, CALIOP is an active sensor onboard the polar-orbiting CALIPSO satellite and is part of the NASA A-Train.

The AVHRR datasets provide cloud top information as global composites with a spatial resolution of  $0.05 \times 0.05^\circ$ , containing data twice per day from ascending and descending for each location. The swath width of AVHRR is wide enough to provide global coverage daily. The AVHRR measurements are used to perform cloud detection and to retrieve cloud top properties, e.g., the top phase, which consists of a binary flag (liquid/ice). Table 1 contains more details about the phase retrieval algorithms. AVHRR-based retrievals often lack sensitivity to high, optically very thin cloud layers, which might be missed or associated with larger uncertainties in the retrieved cloud properties (Stengel et al., 2015).

CALIOP provides vertical distributions of clouds and aerosols along so-called “granules.” A granule is an orbit segment containing cloud, temporal, and geographical information for every vertical profile. The horizontal resolution of CALIPSO is 333 m, while the vertical resolution is 30–60 m. In our analysis we use CALIOP level 2 Cloud Layer Data in version 4.20 with a spatial resolution of 5 km, corresponding to  $\sim 0.05^\circ$  as in AVHRR at the equator. The swath width is very narrow, so that about one month of data must be collected to obtain a near-global coverage. The retrieved cloud phase distinguishes liquid water from “randomly oriented” and “horizontally oriented” ice. Table 1 includes further details on the phase retrieval algorithm. The dataset provides vertical distributions of clouds in layers. Every layer can contain only one thermodynamic phase. CALIOP is able to retrieve up to an optical thickness of approximately 5 into the cloud (Karlsson & Håkansson, 2018). Only “medium” and “high” cloud-aerosol discrimination scores and “medium” and “high” cloud phase confidence scores are used in this study.

### 2.2. Method

We analyzed collocated and non-collocated near-global ( $60^\circ\text{N}$  to  $60^\circ\text{S}$ ) data from June 1, 2009 to May 31, 2013. Using this time period, we benefit from the newest AVHRR/3 instrument onboard the most recent NOAA satellite, avoiding sensor-calibration differences with AVHRR onboard previous satellites leading to potential consistency issues. Moreover, the data in this time period are not biased by the satellite drift yet. Latitudes higher than  $60^\circ$  are excluded from our study because of the data low confidence, due to the low

**Table 1**  
*Cloud Phase Algorithms Used by the Analyzed Datasets*

Dataset	Cloud phase algorithm	Spectral bands ( $\mu\text{m}$ )	Reference
Cloud_cci v2	Cloud types are produced with a threshold decision tree (a series of spectral tests is applied to infrared brightness temperature); then, they are converted to a binary phase. If necessary, cloud top temperature is involved to re-set the phase for $T < -40^\circ\text{C}$ and at $T > 0^\circ\text{C}$	0.6,  1.6/3.75,  10.8,  12	Algorithm Theoretical Baseline Document ATBD-CC4CLv5.1 (2017), Pavlonis and Heidinger (2004), Pavlonis et al. (2005)
Cloud_cci v3	An artificial neural network trained by collocating AVHRR measurements with CALIOP cloud phase produces binary phase information. If necessary, cloud top temperature is involved to re-set the phase at $T < -40^\circ\text{C}$ and at $T > 0^\circ\text{C}$	0.6,  1.6/3.75,  10.8,  12	Algorithm Theoretical Baseline Document ATBD-CC4CLv6.2 (2019), Stengel et al. (2020)
CLARA-A2	As Cloud_cci v2, with some different threshold values in the decision tree scheme	0.6,  1.6/3.75,  10.8,  12	Algorithm Theoretical Baseline Document ATBD-CPP_AVHRR (2016), Pavlonis and Heidinger (2004), Pavlonis et al. (2005)
CALIOP	Cloud altitude is derived as primary product, then converted to temperatures using model data from Goddard Earth Observing System, Version 5 (GEOS-5) vertical profiles. Next, the cloud phase is retrieved using the particulate depolarization ratio of backscattered light (and the cloud top height and temperature, if necessary)	0.532,  1.064	Hu et al. (2009)

solar zenith angle (Grosvenor & Wood, 2014) and the presence of sea ice (King et al., 2004). The collocated data involve pixels retrieved as cloudy by all datasets within 3 minutes and 5 km. As the cloud optical thickness, involved in the cloud type classification, can be detected by the AVHRR sensor only by the channels in the visible range, we consider only daytime measurements, i.e., the ascending track; we do the same for CALIOP to make the comparison as consistent as possible, although daytime CALIOP retrieval has a higher backscatter sensitivity threshold (Winker et al., 2009). We constrain further analyses for latitudinal bands as follows: NH—from  $60^\circ\text{N}$  to  $30^\circ\text{N}$ ; SH—from  $30^\circ\text{S}$  to  $60^\circ\text{S}$ ; Tropics—from  $30^\circ\text{N}$  to  $30^\circ\text{S}$ . Continental and maritime regions are also analyzed. Because only the cloud top information is available from AVHRR, we investigate the cloud top phase distribution in relation to the cloud top temperature, with a focus on the mixed-phase temperature range. With a 4-year analysis, we provide statistics on the supercooled liquid fraction (SLF) in clouds, computed as the ratio between the number of liquid cloud top pixels and the sum of ice plus liquid cloud top pixels. The analyzed isotherms cover the range  $-50^\circ\text{C}$  to  $5^\circ\text{C}$ , with a  $1^\circ\text{C}$  increment. To sort the cloud types, the ISCCP classification (Rossow & Schiffer, 1999) is used, based on threshold values of cloud top pressure (CTP = [0, 440, 680, 1000] hPa) and cloud optical thickness (COT = [0, 3.6, 23, 379]). For simplicity, for each COT-CTP combination the corresponding cloud name (e.g., cirrus, stratocumulus, etc.) assigned in Rossow and Schiffer (1999) is used here, despite being aware that a classification of cloud types purely based on CTP and COT has limitations (Hahn et al., 2001).

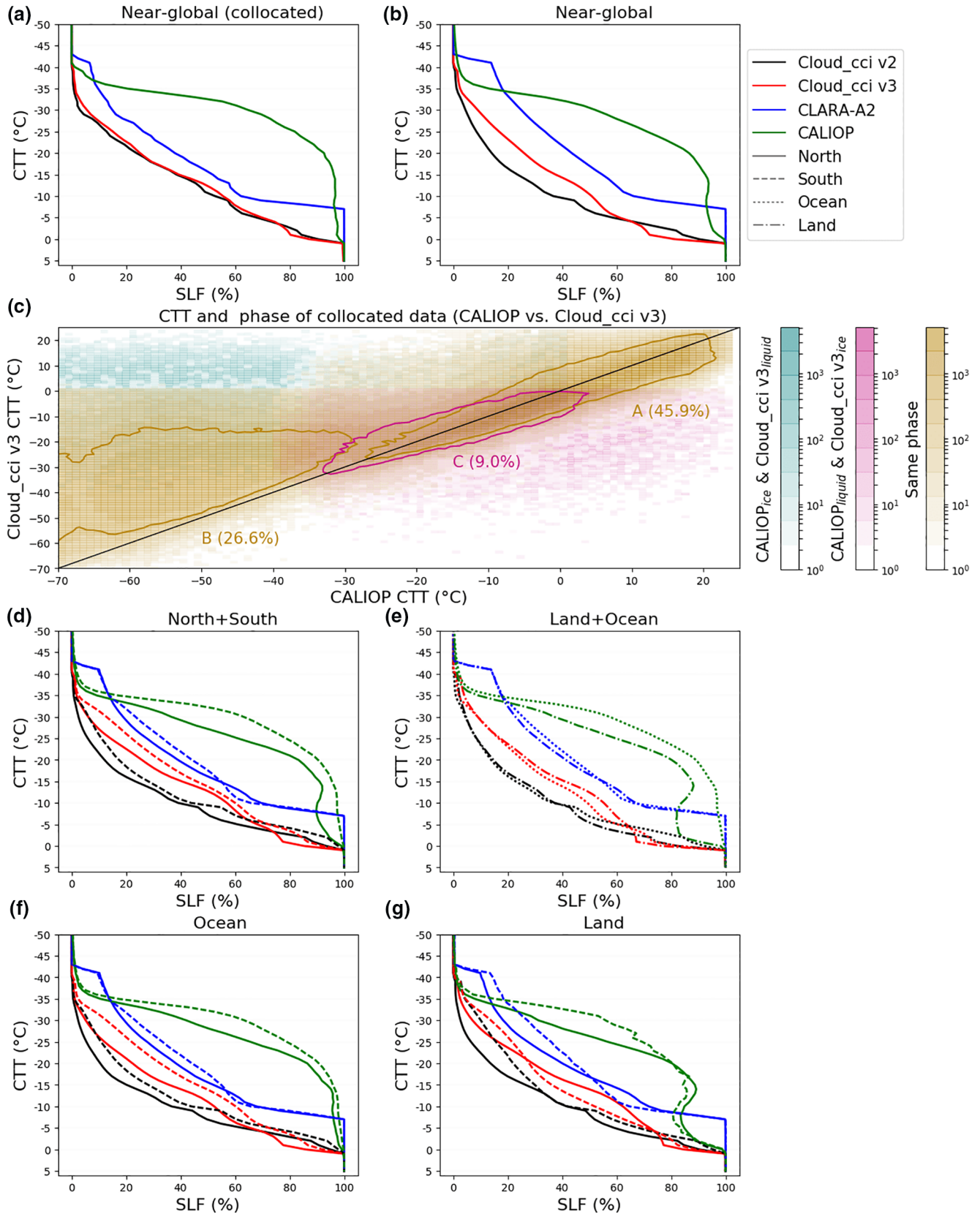
For AVHRR datasets, all the cloudy pixels with  $\text{COT} < 0.3$  are filtered out to improve the data quality (Stengel et al., 2015). To be comparable to the AVHRR datasets and mimic the view of the passive sensor, we remove the uppermost layers from the CALIOP profiles down to an optical thickness of 0.3 and consider the

remaining highest cloud top layer for the study. The cloud classification precedes the computation of SLF on isotherms in the studies in which different cloud types are analyzed.

### 3. Results

As a first step, a comparison between the collocated (Figure 1a) and non-collocated (Figure 1b) data is shown. The difference in SLF and the associated CTT among the datasets stands out in these figures, and in particular the gap between the three AVHRR-based datasets and CALIOP, up to about 25°C or SLF of about 80% at a fixed temperature. In Figure 1c, we show that this disagreement is due to both the CTT and phase retrievals: There is a CTT bias of Cloud\_cci v3 compared to CALIOP mainly at lower temperatures, and a frequent disagreement on phase (with Cloud\_cci v3 retrieving ice where CALIOP retrieves liquid) in the mixed-phase temperature range. This figure uses the collocated data and compares point-by-point the cloud top temperature retrieved by Cloud\_cci v3 and CALIOP over the entire tropospheric temperature range and for three cloud top phase combinations: same phase, CALIOP retrieving ice while Cloud\_cci v3 liquid, and vice versa. The contour lines indicate the areas (A, B, and C) where the frequency of occurrence per 1K × 1K bin is greater than 240. This threshold highlights areas of agreement and disagreement between the datasets, and separate the area where the sensors retrieve the same phase into two regions (A and C) at around  $T = -28^{\circ}\text{C}$ . This temperature value is used to compute the contributions of regions A and C separately. Because of the small contribution given by the collocated pixels with CALIOP retrieving ice and Cloud\_cci v3 liquid, there is no contour line for this phase combination. Region A, including part of the cases with the same phase and representing 45.9% of total cases, does not contribute systematically to the differences in the phase distribution in Figures 1a and 1b, because it incorporates cases with good agreement in temperature and cases where the largest temperature difference is about 10°C. Moreover, only a part of that region is within the mixed-phase temperature range (around 13% of total cases). Conversely, a clear warm bias in Cloud\_cci v3 CTT with respect to CALIOP is indicated in region B, including pixels with the same phase, which represents 26.6% of total cases. This region, albeit including only around 0.7% of total cases between  $-40^{\circ}\text{C}$  and  $0^{\circ}\text{C}$  for both datasets, includes many cases contributing only to the SLF computation for Cloud\_cci v3 (counting about 11% of total cases considering the mixed-phase temperature range for only Cloud\_cci v3), which are excluded from the SLF computation in CALIOP because they are outside its mixed-phase temperature range. Finally, region C, with 9% of total cases (8.7% between  $-40^{\circ}\text{C}$  and  $0^{\circ}\text{C}$ ), refers to pixels retrieved liquid in CALIOP and ice in Cloud\_cci v3. It includes, as region A, cases with good agreement in temperature and cases where the largest difference is about 10°C. Nevertheless, region C contributes principally to the phase mismatch. A point-by-point comparison of CALIOP with CLARA-A2 and with Cloud\_cci v2 (not shown) gives similar results. For AVHRR datasets retrieving liquid while CALIOP retrieving ice, CLARA-A2 revealed more cases than Cloud\_cci v2 and v3 for temperatures below  $-30^{\circ}\text{C}$  and down to  $-41^{\circ}\text{C}$ ; For this reason, CLARA-A2 shows SLF around 7% between  $-40^{\circ}\text{C}$  and  $-41^{\circ}\text{C}$  using the collocated data (Figure 1a) and around 17% using the noncollocated data (Figure 1b). A quantitative analysis of the differences between CALIOP and Cloud\_cci v2 and v3 can be found in Stengel et al. (2020): While any phase bias of Cloud\_cci v2 and v3 with respect to CALIOP has nearly vanished for COTs of  $\sim 0.15$  into the clouds, there is still a significant bias at COT = 1 for the Cloud Top Height (CTH) of ice clouds, to which CTT is linked. As a consequence, CTH is usually retrieved from levels below the levels used to retrieve the phase, so that the retrieved CTT can be warmer than the effective temperature of the assigned cloud top phase, agreeing to our results.

We proceed with the study of SLF in separate geographical regions. Figure 1d shows, for all datasets, larger SLF in SH than in NH (with an average difference for single datasets between 1.7% and 9.8%). In Figure 1e, CALIOP shows clearly larger SLF over ocean than over land (with an average difference of 11.2%), but the AVHRR-based datasets do not agree with CALIOP for the entire temperature range. While larger SLF in SH than in NH is confirmed when constraining the analysis to maritime pixels (Figure 1f, with an average difference for single datasets between 2.1% and 7.3%), it is confirmed only for specific temperature ranges over land (Figure 1g), generally for  $T < -23^{\circ}\text{C}$ . Near-global SLF geographical distributions are shown in Figures S1–S4 in the supporting information.



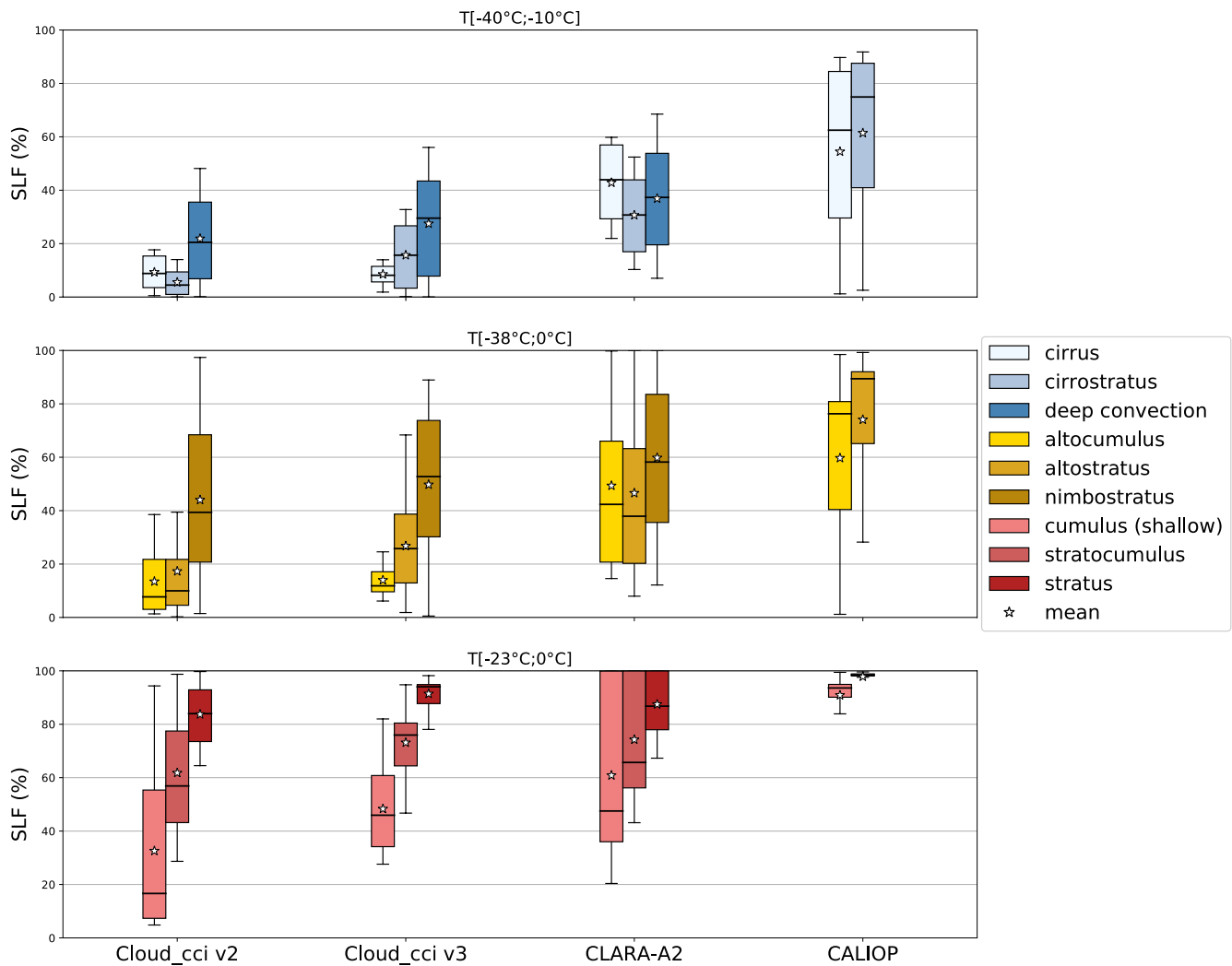


**Figure 2.** Boxplot of the supercooled liquid fraction (SLF) for different cloud types sorted in three height-levels. Clouds at the same height-level share the same cloud top temperature range, specified at the top of each panel. The different datasets are separated by columns and every color corresponds to one cloud type. The boxes extend from the lower to upper quartile values of the data, whereas the whiskers show the entire range of the data. The horizontal lines within the boxes represent the median of the distributions, while the stars represent their mean values.

Next, we investigate the global SLF distribution for different cloud types (Figure 2). The cloud types have been grouped into high-, mid-, and low-level clouds taking into account the temperature ranges that the datasets have in common at the three heights individually. This figure is derived from SLF-CTT distributions, for which the least frequent cases in CTT (frequency of occurrence lower than 2% with respect to the maximum of each distribution in temperature) have been filtered out. Similarly to Figure 1, in Figure 2 the systematically lower SLF in AVHRR compared to CALIOP is found. A further outcome can be identified in this figure for every height-level and almost all cases: the optically thicker the clouds, the larger the SLF. This is consistent in all datasets with a few exceptions.

**Figure 1.** Comparison of supercooled liquid fractions (SLFs) versus cloud top temperature (CTT) for collocated (a) and non-collocated (b) near-global (60°N to 60°S) data, followed by a point-by-point comparison of CTT and cloud top phase for CALIOP and Cloud\_cci v3 using the collocated data (c), where the brightness of the bins (1K × 1K) represents the absolute frequency of occurrence and the different colors represent the different combinations of retrieved phase. The contour lines encompass bins with frequency greater than 240, while the percentages refer to the contoured areas and represent the relative amount of cases within the contour lines with respect to the total cases. A further comparison of SLF versus CTT for non-collocated data follows constraining the extratropical Northern and the Southern Hemispheres (d), land and ocean (e), and extratropical Northern and Southern Hemispheres for only maritime (f) and only continental (g) regions. Different colors in SLF versus CTT plots represent different datasets; different line types represent different regions.

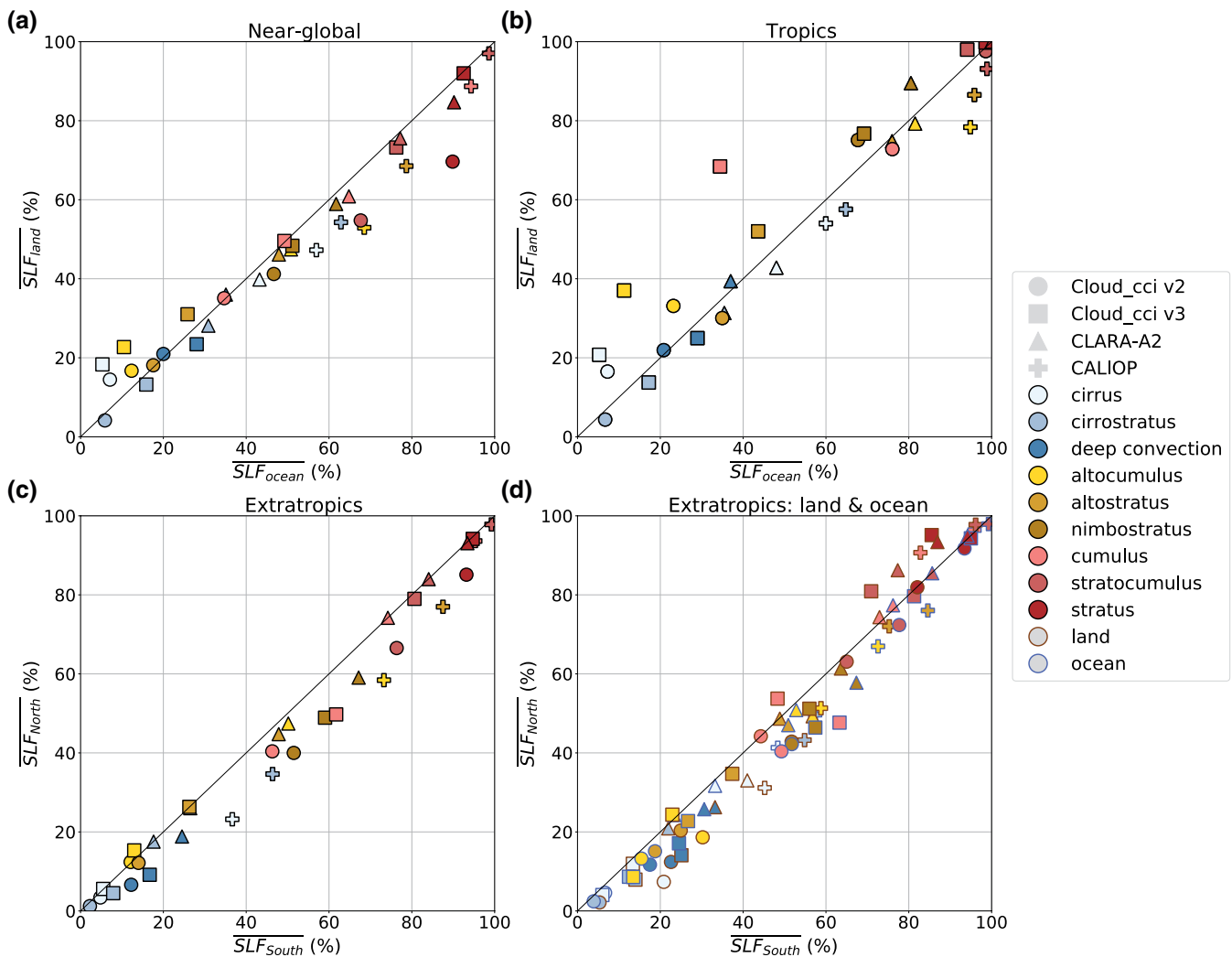


**Figure 3.** Comparison of mean supercooled liquid fraction (SLF) for different cloud types, considered in the temperature ranges they have in common at the same height-level and for each subplot individually, for near-global maritime and continental pixels (a), tropical maritime and continental pixels (b), and extratropical Northern and Southern Hemispheres (c), with the further separation of maritime and continental regions (d). Different markers identify different datasets, filling colors distinguish the cloud types, while edge colors refer to continental or maritime pixels in (d).

Figure 3 condenses the SLF into average values for different cloud types, land and ocean, NH and SH. All datasets confirm generally larger SLF for optically thicker clouds at the same height-level. Figures 3a–3c reveal larger SLF over ocean than over land and in SH than in NH, respectively, for most of the cloud types with the exception of some high- and mid-level clouds in Cloud\_cci v2 and v3, especially in Figure 3a. In the Tropics (Figure 3b), most of the clouds show larger SLF over ocean than over land, except for again some high- and mid-level clouds in Cloud\_cci v2 and v3, and low-level clouds in Cloud\_cci v2. Finally, Figure 3d shows that, separating the maritime and continental pixels in NH and SH, SLF is larger in NH than in SH only for most of the low-level clouds over land (cumulus, stratocumulus, and stratus clouds), otherwise again a larger SLF in SH than NH is found.

This entire study has been conducted using the collocated data too (not shown), confirming the main results of our findings, although with more noise. The collocated data, in fact, represent only about 9.5% of CALIOP and 0.02% of AVHRR non-collocated data.



#### 4. Discussion and Conclusions

We performed a 4-year statistical analysis to better understand the relationship between cloud top phase and temperature in the mixed-phase temperature range ( $-40^{\circ}\text{C}$  to  $0^{\circ}\text{C}$ ). Our study is based on four datasets (Cloud\_cci AVHRR-PM2.0, Cloud\_cci AVHRR-PM3.0, CLARA-A2, and CALIOP v4.20) and consists of the comparison of the retrieved cloud top phase and cloud top temperature in terms of SLF for specific isotherms. The study included collocated data, to determine the inconsistencies among the retrievals, and non-collocated data for the main study. The analysis was conducted from  $60^{\circ}\text{N}$  to  $60^{\circ}\text{S}$ , for extratropical Northern and Southern Hemispheres separately, for the Tropics, for continental and oceanic surfaces, and for different cloud types. To classify the cloud types, cloud top pressure and cloud optical thickness thresholds have been used (Rossow & Schiffer, 1999). Summarizing the main findings:

- Using collocated data, we found a warm bias of AVHRR CTT compared to CALIOP and a phase mismatch (liquid cloud tops in CALIOP retrieved as ice in AVHRR-based datasets). Many factors can contribute to the disagreements between CALIOP and AVHRR. One of the most important ones is the difference of the sensors, the first passive and the second active: While the AVHRR has problems detecting multilayer clouds that include top layers with small COT, leading to misclassifications of cloud top phase, CALIOP can detect multilayer clouds with optical thickness up to 5, and this might cause misclassifications too. Processing the data, cloud edges have not been excluded because it was not possible for the AVHRR-based datasets, representing a possible source of misclassification for low- and mid-level clouds (Pavolonis et al., 2005). Moreover, a possible phase change of a detected cloud top would cause a modification of COT, and therefore a possible misclassification to an optically thicker or thinner cloud category, modifying the SLF of another cloud type. Some of these issues have also been presented in Cesana et al. (2019) for shallow cumulus and stratocumulus clouds, emphasizing that errors in retrieving cloud phase, cloud optical thickness, and cloud top height can result in cloud type misclassifications. Furthermore, the filter we apply to the optical thickness may be not sufficient to make sure that we are analyzing the cloud data in the same way. In Stengel et al. (2015), CALIOP's liquid cloud fraction resulted closer to the AVHRR-based dataset CLAVR-x (Cloud from AVHRR Extended) than to other AVHRR-based datasets. One reason was that for CLAVR-x algorithms a priori information based on CALIOP climatologies was used for ice clouds. This, in turn, prevented that phase and CTT were independently retrieved, a condition required for our study
- We found higher SLF in SH than in NH, in agreement with Tan et al. (2014). This result might be explained by the larger size of the continental area and therefore the prevalence of continental aerosol with the ability to act as INPs in NH. Higher SLF in SH than in NH was found also when constraining the analysis for maritime surfaces, while over-land cases agree on it for temperatures generally colder than  $-23^{\circ}\text{C}$ . Further analyses using different cloud types were necessary to understand the origin of this last feature, principally due to the low-level clouds, which occur at warmer temperatures than the clouds at higher levels. More details are included in the next point
- Analyzing different cloud types and combining NH, SH, continental, and maritime regions, we found higher SLF in SH than in NH (in line with Coopman et al. [2020]), with the exception of the most low-level clouds over land, for which the opposite occurs. This might be due to synoptic conditions or specific aerosol conditions experienced by low-level clouds in those regions and impacting their phase. Considering that the common temperature range of the analyzed continental low-level clouds goes from  $-15^{\circ}\text{C}$  to  $0^{\circ}\text{C}$  (not shown), our result shows agreements with Villanueva et al. (2020), where lower ice content was found in clouds in NH than in SH for  $T = -15^{\circ}\text{C} \pm 6^{\circ}\text{C}$ , probably because of the larger amount of feldspar in SH. Our result could also be explained by the higher density of particles acting as cloud condensation nuclei (CCNs) in NH, resulting in smaller droplet sizes, which might limit secondary ice formation (Mossop, 1980). Our speculations are partially supported by further previous studies: Some anthropogenic aerosols such as black carbon, sulfate, and organic aerosols, do not act as efficient INPs but are efficient CCNs (Hoose & Möhler, 2012); model outputs have shown that sulfate aerosol and black carbon have the highest mass concentration in the lower troposphere of NH (Liu et al., 2009), where they act as CCNs (Boucher & Lohmann, 1995), whereas they act as INPs only at very high altitudes over the Tropics and the polar regions (Liu et al., 2009). Indeed, Tan et al. (2014) found that dust (as mineral desert dust), polluted dust (as dust mixed with urban pollution and biomass burning smoke),

and smoke (as biomass burning aerosols, principally made of soot and organic carbon) are mainly distributed in the Tropics and in NH

- In the analysis of different cloud types, same-height clouds showed SLF increasing with COT. Although clouds containing more droplets than ice particles result in higher optical thickness, we cannot exclude an influence of the cloud dynamics on both COT and SLF. For example, optically thicker clouds tend to have stronger updrafts and consequently higher supersaturation values, which may inhibit the glaciation process (Korolev, 2007), potentially lowering the glaciation temperature in clouds and causing the presence of more supercooled liquid water than ice. From our analysis, it is not possible to determine which process can explain the obtained result

In our study, we have considered possible limitations in the datasets linked to the phase detection of the sensors. Because of this, particular attention has been paid to the cloud optical thickness, bearing in mind that the cloud top phase as well as cloud type might be influenced by it. Despite the differences found in the datasets, our results show broad agreements among them in many aspects, not only proving the robustness of the results but also showing that the passive satellite sensor AVHRR can contribute to the cloud phase research once its limitations have been taken into account. The AVHRR-based datasets can be used for further studies (e.g., for comparison with climate models), benefiting from the long temporal record and good spatial coverage.

### Data Availability Statement

For the used AVHRR-PM data sets, the following DOIs provide additional documentation and data download sites: Cloud\_cci v2—[https://doi.org/10.5676/DWD/ESA\\_Cloud\\_cci/AVHRR-PM/V002](https://doi.org/10.5676/DWD/ESA_Cloud_cci/AVHRR-PM/V002); Cloud\_cci v3—[https://doi.org/10.5676/DWD/ESA\\_Cloud\\_cci/AVHRR-PM/V003](https://doi.org/10.5676/DWD/ESA_Cloud_cci/AVHRR-PM/V003); CLARA-A2—[https://doi.org/10.5676/EUM\\_SAF\\_CM/CLARA\\_AVHRR/V002](https://doi.org/10.5676/EUM_SAF_CM/CLARA_AVHRR/V002). CALIOP data are available online at the NASA Langley Atmospheric Sciences Data Center website (<https://asdc.larc.nasa.gov/>). For the collocated CALIOP data, the CAL\_LID\_L2\_05kmCLay-Prov product was downloaded from the ICARE Data and Service Center (<http://www.icare.univ-lille1.fr>, last access: March 29, 2017).

### Acknowledgments

This project has received funding from the European Research Council (ERC) under the European Union's Horizon 2020 research and innovation programme under Grant Agreement No. 714062 (ERC Starting Grant "C2Phase"). This work was performed on the supercomputer ForHLR funded by the Ministry of Science, Research and the Arts Baden-Württemberg and by the Federal Ministry of Education and Research. The contribution of Martin Stengel was supported by the European Space Agency (ESA) through the Cloud\_cci project (Contract 4000128637/20/I-NB) and by EUMETSAT and its member states through CM SAF. We thank Jan Cermak for the helpful discussions, and the anonymous reviewers for constructive comments on the manuscript.

### References

- ATBD-CC4CLv5.1. (2017). *Algorithm theoretical baseline document ATBD CC4CL—ESA Cloud\_cci [computer software manual]* (Issue 6, Revision: 2). Retrieved from [http://www.esa-cloud-cci.org/?q=documentation\\_v3](http://www.esa-cloud-cci.org/?q=documentation_v3)
- ATBD-CC4CLv6.2 (2019). *Algorithm theoretical baseline document ATBD CC4CL—ESA Cloud\_cci [computer software manual]* (Issue 5, Revision: 1). Retrieved from <http://www.esa-cloud-cci.org/?q=documentation>
- ATBD-CPP\_AVHRR (2016). *Algorithm theoretical baseline document—CM SAF cloud, Albedo, Radiation data record, AVHRR-based, Edition 2 (CLARA-A2)—Cloud Physical products [computer software manual]* (Issue/Revision Index: 2.0). [https://doi.org/10.5676/EUM\\_SAF\\_CM/CLARA\\_AVHRR/V002](https://doi.org/10.5676/EUM_SAF_CM/CLARA_AVHRR/V002)
- Barrett, P. A., Blyth, A., Brown, P. R. A., & Abel, S. J. (2020). The structure of turbulence and mixed-phase cloud microphysics in a highly supercooled altocumulus cloud. *Atmospheric Chemistry and Physics*, 20(4), 1921–1939. <https://doi.org/10.5194/acp-20-1921-2020>
- Boucher, O., & Lohmann, U. (1995). The sulphate-CCN-cloud albedo effect. *Tellus B: Chemical and Physical Meteorology*, 47(3), 281–300. <https://doi.org/10.3402/tellusb.v47i3.16048>
- Cesana, G., Del Genio, A. D., & Chepfer, H. (2019). The cumulus and stratocumulus CloudSat-CALIPSO dataset (CASCCAD). *Earth System Science Data Discussions*, 11, 1–33. <https://doi.org/10.5194/essd-2019-73>
- Cesana, G., & Storelvmo, T. (2017). Improving climate projections by understanding how cloud phase affects radiation. *Journal of Geophysical Research: Atmospheres*, 122, 4594–4599. <https://doi.org/10.1002/2017JD026927>
- Coopman, Q., Hoose, C., & Stengel, M. (2019). Detection of mixed-phase Convective clouds by a binary phase information from the passive Geostationary instrument SEVIRI. *Journal of Geophysical Research: Atmospheres*, 124, 5045–5057. <https://doi.org/10.1029/2018JD029772>
- Coopman, Q., Riedi, J., Zeng, S., & Garrett, T. J. (2020). Space-based analysis of the cloud thermodynamic phase transition for varying microphysical and meteorological regimes. *Geophysical Research Letters*, 47, e2020GL087122. <https://doi.org/10.1029/2020GL087122>
- Costa, A., Meyer, J., Afchine, A., Luebke, A., Günther, G., Dorsey, J. R., et al. (2017). Classification of Arctic, midlatitude and tropical clouds in the mixed-phase temperature regime. *Atmospheric Chemistry and Physics*, 17(19), 12219–12238. <https://doi.org/10.5194/acp-17-12219-2017>
- Forbes, R. M., & Ahlgrimm, M. (2014). On the representation of high-latitude Boundary layer mixed-phase cloud in the ECMWF global model. *Monthly Weather Review*, 142(9), 3425–3445. <https://doi.org/10.1175/MWR-D-13-00325.1>
- Gierens, R., Kneifel, S., Shupe, M. D., Ebell, K., Maturilli, M., & Löhnert, U. (2020). Low-level mixed-phase clouds in a complex arctic environment. *Atmospheric Chemistry and Physics*, 20(6), 3459–3481. <https://doi.org/10.5194/acp-20-3459-2020>
- Grosvenor, D. P., & Wood, R. (2014). The effect of solar zenith angle on MODIS cloud optical and microphysical retrievals within marine liquid water clouds. *Atmospheric Chemistry and Physics*, 14(14), 7291–7321. <https://doi.org/10.5194/acp-14-7291-2014>
- Hahn, C. J., Rossow, W. B., & Warren, S. G. (2001). ISCCP cloud properties associated with standard cloud types identified in individual surface observations. *Journal of Climate*, 14(1), 11–28. [https://doi.org/10.1175/1520-0442\(2001\)014<0011:ICPAWS>2.0.CO;2](https://doi.org/10.1175/1520-0442(2001)014<0011:ICPAWS>2.0.CO;2)

- Henneberger, J., Fugal, J. P., Stetzer, O., & Lohmann, U. (2013). Holimo II: A digital holographic instrument for ground-based in situ observations of microphysical properties of mixed-phase clouds. *Atmospheric Measurement Techniques*, 6(11), 2975–2987. <https://doi.org/10.5194/amt-6-2975-2013>
- Hoose, C., & Möhler, O. (2012). Heterogeneous ice nucleation on atmospheric aerosols: A review of results from laboratory experiments. *Atmospheric Chemistry and Physics*, 12(20), 9817–9854. <https://doi.org/10.5194/acp-12-9817-2012>
- Hu, Y., Winker, D., Vaughan, M., Lin, B., Omar, A., Trepte, C., et al. (2009). CALIPSO/CALIOP cloud phase discrimination algorithm. *Journal of Atmospheric and Oceanic Technology*, 26(11), 2293–2309. <https://doi.org/10.1175/2009JTECHA1280.1>
- Karlsson, K. G., Anttila, K., Trentmann, J., Stengel, M., Fokke Meirink, J., Devasthale, A., et al. (2017). CLARA-A2: The second edition of the CM SAF cloud and radiation data record from 34 years of global AVHRR data. *Atmospheric Chemistry and Physics*, 17(9), 5809–5828. <https://doi.org/10.5194/acp-17-5809-2017>
- Karlsson, K.-G., & Håkansson, N. (2018). Characterization of avhrr global cloud detection sensitivity based on calipso-caliop cloud optical thickness information: Demonstration of results based on the cm saf clara-a2 climate data record. *Atmospheric Measurement Techniques*, 11(1), 633–649. <https://doi.org/10.5194/amt-11-633-2018>
- King, M. D., Platnick, S., Yang, P., Arnold, G. T., Gray, M. A., Riedi, J. C., & Liou, K. N. (2004). Remote sensing of liquid water and ice cloud optical thickness and effective radius in the Arctic: Application of airborne multispectral MAS data. *Journal of Atmospheric and Oceanic Technology*, 21(6), 857–875. [https://doi.org/10.1175/1520-0426\(2004\)021\(0857:RSOLWA\)2.0.CO;2](https://doi.org/10.1175/1520-0426(2004)021(0857:RSOLWA)2.0.CO;2)
- Korolev, A. V. (2007). Limitations of the Wegener-Bergeron-Findeisen mechanism in the evolution of mixed-phase clouds. *Journal of the Atmospheric Sciences*, 64(9), 3372–3375. <https://doi.org/10.1175/JAS4035.1>
- Korolev, A. V. (2008). Rates of phase transformations in mixed-phase clouds. *Quarterly Journal of the Royal Meteorological Society*, 134(632), 595–608. <https://doi.org/10.1002/qj.230>
- Korolev, A. V., McFarquhar, G., Field, P. R., Franklin, C., Lawson, P., Wang, Z., et al. (2017). Mixed-phase clouds: Progress and Challenges. *Meteorological Monographs*, 58, 5.1–5.50. <https://doi.org/10.1175/AMSMONOGRAPHS-D-17-0001.1>
- Liu, Z., Kar, J., Zeng, S., Tackett, J., Vaughan, M., Avery, M., et al. (2019). Discriminating between clouds and aerosols in the CALIOP version 4.1 data products. *Atmospheric Measurement Techniques*, 12(1), 703–734. <https://doi.org/10.5194/amt-12-703-2019>
- Liu, X., Penner, J. E., & Wang, M. (2009). Influence of anthropogenic sulphate and black carbon on upper tropospheric clouds in the NCAR CAM3 model coupled to the IMPACT global aerosol model. *Journal of Geophysical Research*, 114, D03204. <https://doi.org/10.1029/2008JD010492>
- McCoy, D. T., Tan, I., Hartmann, D. L., Zelinka, M. D., & Storelvmo, T. (2016). On the relationships among cloud cover, mixed-phase partitioning, and planetary albedo in GCMs. *Journal of Advances in Modeling Earth Systems*, 8, 650–668. <https://doi.org/10.1002/2015MS000589>
- Mossop, S. C. (1980). The mechanism of ice splinter production during riming. *Geophysical Research Letters*, 7(2), 167–169. <https://doi.org/10.1029/GL007i002p00167>
- Noh, Y.-J., Miller, S. D., Heidinger, A. K., Mace, G. G., Protat, A., & Alexander, S. P. (2019). Satellite-based detection of daytime supercooled liquid-topped mixed-phase clouds over the Southern Ocean using the advanced himawari imager. *Journal of Geophysical Research: Atmospheres*, 124, 2677–2701. <https://doi.org/10.1029/2018JD029524>
- Pavolonis, M. J., & Heidinger, A. K. (2004). Daytime cloud Overlap detection from AVHRR and VIIRS. *Journal of Applied Meteorology*, 43, 762–778. <https://doi.org/10.1175/2099.1>
- Pavolonis, M. J., Heidinger, A. K., & Uttal, T. (2005). Daytime global cloud typing from AVHRR and VIIRS: Algorithm description, validation, and comparisons. *Journal of Applied Meteorology*, 44(6), 804–826. <https://doi.org/10.1175/JAM2236.1>
- Plummer, D. M., Mcfarquhar, G. M., Rauber, R. M., Jewett, B. F., & Leon, D. C. (2014). Structure and statistical analysis of the microphysical properties of generating cells in the comma head region of continental winter cyclones. *Journal of the Atmospheric Sciences*, 71(11), 4181–4203. <https://doi.org/10.1175/JAS-D-14-0100.1>
- Rossow, W. B., & Schiffer, R. A. (1999). Advances in understanding clouds from ISCCP. *Bulletin of the American Meteorological Society*, 80(11), 2261–2287. [https://doi.org/10.1175/1520-0477\(1999\)080<2261:AIUCFJ>2.0.CO;2](https://doi.org/10.1175/1520-0477(1999)080<2261:AIUCFJ>2.0.CO;2)
- Stengel, M., Mieruch, S., Jerg, M., Karlsson, K. G., Scheirer, R., Maddux, B., et al. (2015). The Clouds Climate Change Initiative: Assessment of state-of-the-art cloud property retrieval schemes applied to AVHRR heritage measurements. *Remote Sensing of Environment*, 162, 363–379. <https://doi.org/10.1016/j.rse.2013.10.035>
- Stengel, M., Stapelberg, S., Sus, O., Finkensieper, S., Würzler, B., Philipp, D., et al. (2020). Cloud\_cci advanced very high resolution radiometer post meridiem (avhrr-pm) dataset version 3: 35-year climatology of global cloud and radiation properties. *Earth System Science Data*, 12(1), 41–60. <https://doi.org/10.5194/essd-12-41-2020>
- Stengel, M., Stapelberg, S., Sus, O., Schlundt, C., Poulsen, C., Thomas, G., et al. (2017). Cloud property datasets retrieved from AVHRR, MODIS, AATSR and MERIS in the framework of the Cloud-cci project. *Earth System Science Data*, 9(2), 881–904. <https://doi.org/10.5194/essd-9-881-2017>
- Tan, I., Oreopoulos, L., & Cho, N. (2019). The role of thermodynamic phase shifts in cloud optical depth variations with temperature. *Geophysical Research Letters*, 46, 4502–4511. <https://doi.org/10.1029/2018GL081590>
- Tan, I., Storelvmo, T., & Choi, Y. S. (2014). Spaceborne lidar observations of the ice-nucleating potential of dust, polluted dust, and smoke aerosols in mixed-phase clouds. *Journal of Geophysical Research: Atmospheres*, 119, 6653–6665. <https://doi.org/10.1002/2013JD021333>
- Villanueva, D., Heinold, B., Seifert, P., Deneke, H., Radenz, M., & Tegen, I. (2020). The day-to-day co-variability between mineral dust and cloud glaciation: A proxy for heterogeneous freezing. *Atmospheric Chemistry and Physics*, 20(4), 2177–2199. <https://doi.org/10.5194/acp-20-2177-2020>
- Wang, Z., French, J., Vali, G., Wechsler, P., Haimov, S., Rodi, A., et al. (2012). Single aircraft integration of remote sensing and in situ sampling for the study of cloud microphysics and dynamics. *Bulletin of the American Meteorological Society*, 93(5), 653–668. <https://doi.org/10.1175/BAMS-D-11-00044.1>
- Winker, D. M., Vaughan, M. A., Omar, A., Hu, Y., Powell, K. A., Liu, Z., et al. (2009). Overview of the CALIPSO mission and CALIOP data processing algorithms. *Journal of Atmospheric and Oceanic Technology*, 26(11), 2310–2323. <https://doi.org/10.1175/2009JTECHA1281.1>
- Yu, G., Verlinde, J., Clothiaux, E. E., & Chen, Y.-S. (2014). Mixed-phase cloud phase partitioning using millimeter wavelength cloud radar Doppler velocity spectra. *Journal of Geophysical Research: Atmospheres*, 119, 7556–7576. <https://doi.org/10.1002/2013JD021182>
- Zhang, D., Wang, Z., & Liu, D. (2010). A global view of midlevel liquid-layer topped stratiform cloud distribution and phase partition from calipso and cloudsat measurements. *Journal of Geophysical Research: Atmospheres*, 115, D03205. <https://doi.org/10.1029/2009JD012143>